Evidence for quadratic tidal tensor bias from the halo bispectrum

Tobias Baldauf,[1,][*] Uroš Seljak,[1,2,3,4] Vincent Desjacques,[5] and Patrick McDonald[2,6]

[1]*Institute for Theoretical Physics, University of Zurich, Zurich, Switzerland*
[2]*Lawrence Berkeley National Laboratory, Berkeley, California, USA*
[3]*Physics Department and Astronomy Department, University of California, Berkeley, California, USA*
[4]*Institute for the Early Universe, EWHA Womans University, Seoul, South Korea*
[5]*Department of Theoretical Physics and Center for Astroparticle Physics, University of Geneva, Geneva, Switzerland*
[6]*Physics Department, Brookhaven National Laboratory, Upton, New York, USA*

The relation between the clustering properties of luminous matter in the form of galaxies and the underlying dark matter distribution is of fundamental importance for the interpretation of ongoing and upcoming galaxy surveys. The so-called local bias model, where galaxy density is a function of local matter density, is frequently discussed as a means to infer the matter power spectrum or correlation function from the measured galaxy correlation. However, gravitational evolution generates a term quadratic in the tidal tensor and thus nonlocal in the Eulerian density field, even if this term is absent in the initial conditions (Lagrangian space). Because the term is quadratic, it contributes as a loop correction to the power spectrum, so the standard linear bias picture still applies on very large scales; however, it contributes at leading order to the bispectrum for which it is significant on all scales. Such a term could also be present in Lagrangian space if halo formation were influenced by the tidal field. We measure the corresponding coupling strengths from the matter-matter-halo bispectrum in numerical simulations and find a nonvanishing coefficient for the tidal tensor term. We find no scale dependence of the inferred bias parameters up to $k \sim 0.1 h$ Mpc^{-1} and that the tidal effect is increasing with halo mass. While the local Lagrangian bias picture is a better description of our results than the local Eulerian bias picture, our results suggest that there might be a tidal tensor bias already in the initial conditions. We also find that the coefficients of the quadratic density term deviate quite strongly from the theoretical predictions based on the spherical collapse model and a universal mass function. Both quadratic density and tidal tensor bias terms must be included in the modeling of galaxy clustering of current and future surveys if one wants to achieve the high precision cosmology promise of these data sets.

I. INTRODUCTION

Large-scale structure (LSS), the large-scale distribution of matter in the Universe, contains a wealth of information about the history and composition of the Universe as well as fundamental physics. For instance, LSS has the potential to constrain neutrino masses or modifications of gravity, which however requires percent level accuracy for the theory and observations. Besides gravitational lensing, which is sensitive to the total matter distribution, the positions of galaxies are the main observable and tool to infer the underlying matter distribution. They have the advantage of higher statistical power relative to weak lensing surveys. Ongoing and upcoming LSS surveys such as BOSS, BigBOSS, EUCLID, and DES will provide an unprecedented quality of galaxy clustering data, which needs to be properly analyzed.

A crucial step in the analysis of galaxy surveys is to connect the distribution of the tracer to the underlying distribution of matter. The first step in this logical chain is the realization that galaxies form preferentially in the potential wells of collapsed dark matter halos, where the hot gas can cool sufficiently fast [1,2]. This leads to the question of how the clustering properties of dark matter halos relate to the clustering of matter in general. The answer to this question is usually phrased in terms of a relation between the overdensities in these two fields and is dubbed a halo biasing scheme. With the ever increasing computing power it is in principle possible to generate templates for the survey analysis for standard ΛCDM and even modified gravity models using *N*-body simulations. This approach becomes very expensive when it is to be used in Markov-chain-Monte Carlo parameter inference methods and does not provide insight into the underlying clustering properties. We thus consider it important to understand the properties of halo clustering by testing theoretical prescriptions on simulations with the final goal of devising *analytical* and thus easily evaluable models for the survey analysis.

The so-called local biasing model [3,4], where galaxy and halo density is a function of local matter density, has been the most popular model used in previous work. In the simplest version one adds another contribution that scales quadratically with density, the quadratic density bias term.

[*]baldauf@physik.uzh.ch

Recent work has argued, based on symmetry and analyticity arguments, that there are additional terms not included in the local bias model that appear in the power spectrum and are formally at the same order as that of quadratic bias [5]. One of these terms is quadratic in density but nonlocal and can be written as the square of the tidal tensor. The first goal of this paper is to provide additional theoretical motivation for inclusion of this term in the analysis of galaxy clustering.

The working horses in LSS analysis are the two-point functions, the correlation function and the power spectrum. Purely Gaussian, linear fields are completely characterized by their two-point function. However, nonlinear phenomena in galaxy and halo formation as well as nonlinear gravitational clustering can generate the full hierarchy of n-point functions. These higher-order statistics might be difficult to measure in the sky due to nontrivial survey windows and redshift space distortions, but they can be easily extracted from N-body simulations. The simplest statistic beyond the power spectrum is the bispectrum

$$\langle \delta(\boldsymbol{k}_1)\delta(\boldsymbol{k}_2)\delta(\boldsymbol{k}_3)\rangle = B(\boldsymbol{k}_1, \boldsymbol{k}_2, \boldsymbol{k}_3)(2\pi)^3\delta^{(\mathrm{D})}(\boldsymbol{k}_1 + \boldsymbol{k}_2 + \boldsymbol{k}_3),$$

(1)

which is well suited for the study of next-to-leading-order effects in cosmic density fields [6–10]. While these contribute only loop terms to the power spectrum they are the leading-order terms for the bispectrum, which vanishes for purely linear Gaussian fields.

The second aim of this study is to probe the halo bispectrum for Gaussian initial conditions in the low-k regime, in order to extract the two terms that lead to a quadratic coupling between the number density of collapsed objects and the long wavelength matter fluctuations, quadratic density bias and quadratic tidal tensor bias. We present a study of their scale and mass dependence using N-body simulations and we compare the numerical results to the theoretical expectations based on simple halo bias models.

This paper is organized as follows. In Sec. II, we review the standard formulation of the bias model and discuss possible extensions. Section III describes the simulations, the bispectrum measurement and data reduction as well as the parameter estimation. The results are presented in Sec. IV. Finally, in Sec. V we discuss our findings and their implications as well as possible directions for future investigation.

II. THE BIAS MODEL: LOCAL AND NONLOCAL FORMS

A. Standard formulation: Local bias

The formation of galaxies and their host dark matter halos is a complicated highly nonperturbative process. It is, however, reasonable to assume that certain properties of collapsed objects, for instance their number density, are related to the coarse grained underlying matter density field in the same region of space. Neglecting complications arising from gas physics, the number density of collapsed objects can be written as a functional of the underlying matter density perturbation [4]

$$\delta_{\mathrm{h}}(\boldsymbol{x}, \eta) = \mathcal{F}[\delta(\boldsymbol{x}', \eta)].$$

(2)

On large scales, this functional is commonly approximated by a *local* and *linear* bias model $\delta_{\mathrm{h}}(\boldsymbol{x}, \eta) = b_1\delta(\boldsymbol{x}, \eta)$ (plus generally a noise term which we will avoid in this paper by only looking at cross correlations with mass). The next step is to give up on linearity and to introduce the second-order local bias model $\delta_{\mathrm{h}}(\boldsymbol{x}, \eta) = b_1\delta(\boldsymbol{x}, \eta) + b_2\delta^2(\boldsymbol{x}, \eta)$. This model has been well studied in the literature in combination with standard perturbation theory (SPT) and leads to nontrivial renormalizations of the leading-order bias parameter [11]. Measurements of the quadratic bias parameters of this model in the two-point function [12] and three-point function [10,13] have lead to contradictory results, which raises doubts about the completeness of the model.

B. Tidal terms

The power series expansion of the functional presented above is certainly overly simplified and one should consider whether other terms could influence the number density of collapsed objects. As proposed in Ref. [5], the environmental dependence of halo formation could lead to a dependence on the tidal field, as quantified by the tidal tensor

$$s_{ij}(\boldsymbol{x}, \eta) = \partial_i\partial_j\Phi(\boldsymbol{x}, \eta) - \frac{1}{3}\delta^{(\mathrm{K})}_{ij}\delta(\boldsymbol{x}, \eta).$$

(3)

Note that we absorbed the constants in the Poisson equation into the gravitational potential $\boldsymbol{\nabla}^2\Phi(\boldsymbol{x}, \eta) = \delta(\boldsymbol{x}, \eta)$ and subtract out the trace from the tidal tensor because it is degenerate with the density field. The corresponding expression in Fourier space is given by

$$s_{ij}(\boldsymbol{k}, \eta) = \left(\frac{k_ik_j}{k^2} - \frac{1}{3}\delta^{(\mathrm{K})}_{ij}\right)\delta(\boldsymbol{k}, \eta).$$

(4)

The halo overdensity is a scalar quantity and can thus only depend on scalars. The simplest scalar that can be constructed from the tidal tensor is given by $s^2(\boldsymbol{x}) = s_{ij}(\boldsymbol{x})s_{ij}(\boldsymbol{x})$ which in Fourier space is expressed by the convolution

$$s^2(\boldsymbol{k}, \eta) = \int \frac{\mathrm{d}^3k'}{(2\pi)^3} S_2(\boldsymbol{k}', \boldsymbol{k} - \boldsymbol{k}')\delta(\boldsymbol{k}', \eta)\delta(\boldsymbol{k} - \boldsymbol{k}', \eta),$$

(5)

where we have implicitly defined the kernel

$$S_2(\boldsymbol{q}_1, \boldsymbol{q}_2) = \frac{(\boldsymbol{q}_1 \cdot \boldsymbol{q}_2)^2}{q_1^2 q_2^2} - \frac{1}{3}.$$

(6)

Following Ref. [5], the halo density field up to second order can be written as

$$\delta_{\rm h}(\boldsymbol{x}, \eta) = b_1 \delta(\boldsymbol{x}, \eta) + b_2[\delta^2(\boldsymbol{x}, \eta) - \langle \delta^2(\boldsymbol{x}, \eta) \rangle]$$
$$+ b_{s^2}[s^2(\boldsymbol{x}, \eta) - \langle s^2(\boldsymbol{x}, \eta) \rangle], \tag{7}$$

where we absorbed prefactors of $1/2$ into the bias parameters. We truncated the series at second order, since higher-order terms influence the bispectrum only through loop corrections, which are believed to be subdominant on large scales. As can be easily verified from the above definitions one has $\langle s^2(\boldsymbol{x}, \eta) \rangle = 2/3 \langle ^{(1)}\delta^2(\boldsymbol{x}, \eta) \rangle$.

C. Lagrangian bias

In the usual Lagrangian bias picture, the galaxy formation sites are identified in the primordial density field, and it is assumed that the primordial halo density field at initial time $\eta_{\rm i}$ can be written as a power series in the primordial matter fluctuations. For calculational convenience, the expansion can be rewritten in terms of the linearly extrapolated density field $\delta(\boldsymbol{q}, \eta) = D(\eta)/D(\eta_i)\delta(\boldsymbol{q})$:

$$\delta_{\rm h}(\boldsymbol{q}) = \sum_l \frac{b_l^{(\rm L)}(\eta_{\rm i})}{l!}[\delta^l(\boldsymbol{q}) - \langle \delta^l(\boldsymbol{q}) \rangle]$$
$$= \sum_l \frac{b_l^{(\rm L)}(\eta)}{l!}[\delta^l(\boldsymbol{q}, \eta) - \langle \delta^l(\boldsymbol{q}, \eta) \rangle], \tag{8}$$

where $b_l^{(\rm L)}(\eta) = (D(\eta_i)/D(\eta))^l b_l^{(\rm L)}(\eta_i)$ and $\boldsymbol{q}$ is the Lagrangian position. Here, we introduced the conformal time $ad\eta = dt$ and the linear growth factor $D(\eta)$, normalized to unity at present time. We start the sum from $l = 1$ because the $l = 0$ term vanishes by requiring that the halo field has a vanishing mean. In contrast to this, the Eulerian bias model expands the halo density field at a certain point in time in the nonlinear matter density field at the same time. Motivation for a Lagrangian nature of halo bias comes from the peak model [14–17], where the peaks of the primordial density field are associated with the formation sites of protohalos.

It now remains to connect the Lagrangian density fields to the observable Eulerian ones. The continuity equation for halos requires

$$[1 + \delta_{\rm h}(\boldsymbol{x}, \eta)]d^3 x = [1 + \delta_{\rm h}(\boldsymbol{q})]d^3 q, \tag{9}$$

where

$$[1 + \delta(\boldsymbol{x}, \eta)]d^3 x = d^3 q \tag{10}$$

is the continuity equation for the underlying dark matter field. Note that the Lagrangian density field we work with is always the linear density field, because this was the definition of the bias expansion in Eq. (8)—more general expansions are possible in principle.

The Lagrangian and Eulerian positions are related by $\boldsymbol{x}(\boldsymbol{q}, \eta) = \boldsymbol{q} + \boldsymbol{\psi}(\boldsymbol{q}, \eta)$, thus up to third order in the density field we have

$$\delta(\boldsymbol{q}) = \delta(\boldsymbol{x}, \eta) - \Psi_i(\boldsymbol{q}, \eta)\partial_i \delta(\boldsymbol{q})$$
$$+ \frac{1}{2}\Psi_i(\boldsymbol{q}, \eta)\Psi_j(\boldsymbol{q}, \eta)\partial_i \partial_j \delta(\boldsymbol{q}). \tag{11}$$

In contrast to Eulerian perturbation theory, where the density is the central quantity, Lagrangian perturbation theory (LPT) has the displacement field $\boldsymbol{\psi}$ as the central dynamic quantity and the density fields are only derived quantities (for the basics of LPT and its relation to SPT see Appendix A). For simplicity, we will focus on the matter-only Einstein–de Sitter universe for the theoretical calculations throughout this paper. Considering more realistic ΛCDM growth rates in the PT expressions typically leads to subpercent level changes in the final results and does not change the qualitative behavior [18]. Using the Lagrangian bias expansion (8) in (9) and expressing the Lagrangian position field in terms of the Eulerian position, we have (see also Ref. [19])

$$\delta_{\rm h}(\boldsymbol{x}, \eta) = [1 + b_1^{(\rm L)}(\eta)]^{(1)}\delta(\boldsymbol{x}, \eta) + b_1^{(\rm L)}(\eta)\delta^2(\boldsymbol{x}, \eta)$$
$$+ \frac{1}{2}b_2^{(\rm L)}(\eta)[^{(1)}\delta^2(\boldsymbol{x}, \eta) - \langle ^{(1)}\delta^2(\boldsymbol{x}, \eta) \rangle]$$
$$- b_1^{(\rm L)}(\eta)\boldsymbol{\psi}(\boldsymbol{q}, \eta) \cdot \boldsymbol{\nabla}\delta(\boldsymbol{x}, \eta) + {}^{(2)}\delta(\boldsymbol{x}, \eta). \tag{12}$$

Reorganizing the terms in order to have the first-order bias multiply the full second-order matter density field, we obtain

$$\delta_{\rm h}(\boldsymbol{x}, \eta) = [1 + b_1^{(\rm L)}(\eta)][^{(1)}\delta(\boldsymbol{x}, \eta) + {}^{(2)}\delta(\boldsymbol{x}, \eta)]$$
$$+ \left(\frac{4}{21}b_1^{(\rm L)} + \frac{1}{2}b_2^{(\rm L)}(\eta)\right)$$
$$\times [^{(1)}\delta^2(\boldsymbol{x}, \eta) - \langle ^{(1)}\delta^2(\boldsymbol{x}, \eta) \rangle]$$
$$- \frac{2}{7}b_1^{(\rm L)}(\eta)[s^2(\boldsymbol{x}, \eta) - \langle s^2(\boldsymbol{x}, \eta) \rangle], \tag{13}$$

where we used that the second-order mass density (in SPT and LPT) can be written in configuration space as (see e.g., Ref. [20])

$${}^{(2)}\delta(\boldsymbol{x}, \eta) = \frac{17}{21}{}^{(1)}\delta^2(\boldsymbol{x}, \eta) - \boldsymbol{\psi}(\boldsymbol{x}, \eta) \cdot \boldsymbol{\nabla}\delta(\boldsymbol{x}, \eta) + \frac{2}{7}s^2(\boldsymbol{x}, \eta). \tag{14}$$

We see that the functional form of the above result agrees with Eq. (7), but complements it with a dynamical perspective. In particular, we see that even in the absence of a tidal tensor bias in the initial conditions, such a term will be generated by subsequent gravitational evolution. While our result in Eq. (13) is consistent with the relations presented in Ref. [19], we have reorganized terms in order to have the first-order bias multiplying the second-order density field equation (14) and to make the formal equivalence with the phenomenological picture presented above more obvious. Furthermore, there are no $b_0^{(\rm L)}$ factors, because we fixed the original Taylor series for $\delta_{\rm h}(\boldsymbol{q})$ to have a vanishing mean.

D. Coevolution of halos and dark matter

In this subsection, we will consider an (at first glance) Eulerian approach to halo clustering and consider the coevolution of the coupled halo-dark matter fluid (for a similar approach in combination with resummed perturbation theory see Ref. [21]). Assuming vanishing velocity bias $\boldsymbol{v}_h = \boldsymbol{v}$ and *conservation of halo number*, we can write down a coupled system of differential equations for the matter and halo fluid [22], namely the continuity equation for halos, the continuity equation for the matter and the combined Euler and Poisson equations for matter

$$\delta'_h(\boldsymbol{k}, \eta) + \theta(\boldsymbol{k}, \eta) = -\int \frac{d^3 k'}{(2\pi)^3} \alpha(\boldsymbol{k}', \boldsymbol{k} - \boldsymbol{k}') \theta(\boldsymbol{k}', \eta)$$
$$\times \delta_h(\boldsymbol{k} - \boldsymbol{k}', \eta), \qquad (15)$$

$$\delta'(\boldsymbol{k}, \eta) + \theta(\boldsymbol{k}, \eta) = -\int \frac{d^3 k'}{(2\pi)^3} \alpha(\boldsymbol{k}', \boldsymbol{k} - \boldsymbol{k}')$$
$$\times \theta(\boldsymbol{k}', \eta) \delta(\boldsymbol{k} - \boldsymbol{k}', \eta), \qquad (16)$$

$$\theta'(\boldsymbol{k}, \eta) + \mathcal{H}(\eta) \theta(\boldsymbol{k}, \eta) + \frac{3}{2} \Omega_m(\eta) \mathcal{H}^2(\eta) \delta(\boldsymbol{k}, \eta)$$
$$= -\int \frac{d^3 k'}{(2\pi)^3} \beta(\boldsymbol{k}', \boldsymbol{k} - \boldsymbol{k}') \theta(\boldsymbol{k}', \eta) \theta(\boldsymbol{k} - \boldsymbol{k}', \eta) \qquad (17)$$

with

$$\alpha(\boldsymbol{q}_1, \boldsymbol{q}_2) = \frac{(\boldsymbol{q}_1 + \boldsymbol{q}_2) \cdot \boldsymbol{q}_1}{q_1^2},$$
$$\beta(\boldsymbol{q}_1, \boldsymbol{q}_2) = \frac{1}{2}(\boldsymbol{q}_1 + \boldsymbol{q}_2)^2 \frac{\boldsymbol{q}_1 \cdot \boldsymbol{q}_2}{q_1^2 q_2^2}. \qquad (18)$$

Here we introduced the velocity divergence $\theta(\boldsymbol{x}) = \nabla \cdot \boldsymbol{v}(\boldsymbol{x})$. The matter equations at first order are solved by $^{(1)}\theta(\boldsymbol{k}, \eta) = -\mathcal{H}(\eta) {}^{(1)}\delta(\boldsymbol{k}, \eta)$ and $^{(1)}\delta(\boldsymbol{k}, \eta) = D(\eta) {}^{(1)}\delta_0(\boldsymbol{k})$, where $^{(1)}\delta_0(\boldsymbol{k})$ is the present day linear overdensity. The second-order solution for the matter yields

$$^{(2)}\delta(\boldsymbol{k}, \eta) = \int \frac{d^3 k'}{(2\pi)^3} F_2(\boldsymbol{k}', \boldsymbol{k} - \boldsymbol{k}') {}^{(1)}\delta(\boldsymbol{k}', \eta) {}^{(1)}\delta(\boldsymbol{k} - \boldsymbol{k}', \eta),$$
$$(19)$$

$$^{(2)}\theta(\boldsymbol{k}, \eta) = -\mathcal{H}(\eta) \int \frac{d^3 k'}{(2\pi)^3}$$
$$\times G_2(\boldsymbol{k}', \boldsymbol{k} - \boldsymbol{k}') {}^{(1)}\delta(\boldsymbol{k}', \eta) {}^{(1)}\delta(\boldsymbol{k} - \boldsymbol{k}', \eta),$$
$$(20)$$

where the second-order SPT mode coupling kernels are defined as [23]

$$F_2(\boldsymbol{q}_1, \boldsymbol{q}_2) = \frac{5}{7}\alpha(\boldsymbol{q}_1, \boldsymbol{q}_2) + \frac{2}{7}\beta(\boldsymbol{q}_1, \boldsymbol{q}_2), \qquad (21)$$

$$G_2(\boldsymbol{q}_1, \boldsymbol{q}_2) = \frac{3}{7}\alpha(\boldsymbol{q}_1, \boldsymbol{q}_2) + \frac{4}{7}\beta(\boldsymbol{q}_1, \boldsymbol{q}_2). \qquad (22)$$

The first-order equation for the halos can be solved using the local bias ansatz $^{(1)}\delta_h(\boldsymbol{k}, \eta) = b_1^{(E)}(\eta) {}^{(1)}\delta(\boldsymbol{k}, \eta)$, which then gives the time evolution of the first-order bias as

$$\frac{b_1^{(E)}(\eta) - 1}{b_1^{(E)}(\eta_i) - 1} = \frac{D(\eta_i)}{D(\eta)}. \qquad (23)$$

This relation is known as debiasing; i.e., at late times the bias converges to unity and the halo and matter density field agree [24].

Solving Eq. (15) at second order using the second-order matter solutions, we obtain

$$^{(2)}\delta_h(\boldsymbol{k}, \eta) = {}^{(2)}\delta_h(\boldsymbol{k}, \eta_i) + b_1^{(E)}(\eta) \int \frac{d^3 k'}{(2\pi)^3} F_2(\boldsymbol{k}', \boldsymbol{k} - \boldsymbol{k}')$$
$$\times \delta(\boldsymbol{k}', \eta) \delta(\boldsymbol{k} - \boldsymbol{k}', \eta)$$
$$+ \frac{4}{21}(b_1^{(E)}(\eta) - 1) \int \frac{d^3 k'}{(2\pi)^3} \delta(\boldsymbol{k}', \eta) \delta(\boldsymbol{k} - \boldsymbol{k}', \eta)$$
$$- \frac{2}{7}(b_1^{(E)}(\eta) - 1) \int \frac{d^3 k'}{(2\pi)^3} S_2(\boldsymbol{k}', \boldsymbol{k} - \boldsymbol{k}')$$
$$\times \delta(\boldsymbol{k}', \eta) \delta(\boldsymbol{k} - \boldsymbol{k}', \eta), \qquad (24)$$

where we assumed $D(\eta_i) \ll D(\eta)$. Here, we have isolated the part proportional to the second-order matter field in the first line. Thus, the dynamical evolution naturally introduces a $\delta^2(\boldsymbol{x})$ and a $s^2(\boldsymbol{x})$ term, even in the absence thereof at some initial time η_i. Translating back to real space, we see that this has the same functional form as Eq. (7) and agrees with the Lagrangian bias picture. The equivalence is even more obvious if we have $^{(2)}\delta_h(\boldsymbol{x}, \eta_i) = b_2^{(L)}(\eta_i) {}^{(1)}\delta^2(\boldsymbol{x}, \eta_i)/2 = b_2^{(L)}(\eta) {}^{(1)}\delta^2(\boldsymbol{x}, \eta)/2$ in correspondence to the Lagrangian bias picture discussed above (see the next subsection for a relation between the parameters of the models discussed here). We note in retrospect that, while the calculation took an Eulerian form, the specification that galaxies formed at an early time tracing the initial density field (or at least the location where they will form is determined this way) and then just follow gravity is actually the same one made in the Lagrangian calculation.

E. Relation between Eulerian and Lagrangian bias parameters

As we have seen above, the Lagrangian bias model, the coevolution model and the educated guess of Ref. [5] all lead to the same functional form for the halo density field if one identifies the parameters of the model as

$$b_1 = b_1^{(E)}(\eta) = 1 + b_1^{(L)}(\eta), \qquad (25)$$

$$b_2 = \frac{1}{2} b_2^{(E)}(\eta) = \frac{4}{21} b_1^{(L)}(\eta) + \frac{1}{2} b_2^{(L)}(\eta). \qquad (26)$$

This identification agrees with the one of the spherical collapse picture [25]. Note however that our results are

not relying on the spherical collapse dynamics. For the prefactor of the tidal field scalar we have

$$b_{s^2} = -\frac{2}{7}(b_1^{(E)}(\eta) - 1) = -\frac{2}{7}b_1^{(L)}(\eta). \quad (27)$$

In this model, there is no tidal field bias in Lagrangian space, consistent with the spherical collapse model, although in the ellipsoidal collapse model [26–29] such a term would be allowed.

When comparing our measurements to theoretical bias models, we consider the bias derived from the Sheth-Tormen [30] mass function with parameters $p = 0.15$ and $q = 0.75$ that were shown to be in good agreement with first-order bias in N-body simulations [31], although we checked that the predictions do not differ much from those using the original values in Ref. [30]. The Lagrangian bias parameters are then given by the first and second derivatives of the mass function $n(M)$ with respect to a long wavelength background fluctuation δ_1. For universal mass functions these can be rewritten as derivatives with respect to the peak height $\nu(M, \eta) = \delta_c^2/\sigma^2(M, \eta)$:

$$b_1^{(L)} = \frac{1}{\bar{n}}\frac{\partial n}{\partial \delta_1} = -\frac{1}{\bar{n}}\frac{2\nu}{\delta_c}\frac{\partial n}{\partial \nu}, \quad (28)$$

$$b_2^{(L)} = \frac{1}{\bar{n}}\frac{\partial^2 n}{\partial \delta_1^2} = \frac{4}{\bar{n}}\frac{\nu^2}{\delta_c^2}\frac{\partial^2 n}{\partial \nu^2} + \frac{2}{\bar{n}}\frac{\nu}{\delta_c^2}\frac{\partial n}{\partial \nu}, \quad (29)$$

where $\delta_c = 1.686$ is the critical density for spherical collapse. The derivatives of the Sheth-Tormen mass function read

$$\frac{1}{n}\frac{\partial n}{\partial \nu} = -\frac{q\nu - 1}{2\nu} - \frac{p}{\nu(1 + (q\nu)^p)}, \quad (30)$$

$$\frac{1}{n}\frac{\partial^2 n}{\partial \nu^2} = \frac{p^2 + \nu pq}{\nu^2(1 + (q\nu)^p)} + \frac{(q\nu)^2 - 2q\nu - 1}{4\nu^2}. \quad (31)$$

The mass dependence of the bias function is presented in Fig. 4 and discussed in Sec. IV.

F. Bispectra

The leading-order contribution to the bispectrum arises from quadratic terms in the fields. Higher-order couplings enter only through loop corrections, which gain importance for high k. This is equivalent to the situation in the power spectrum, where linear terms in the field are dominant on large scales and loop corrections from quadratic and higher-order terms gain importance for high k.

The tree-level matter bispectrum in SPT is given by

$$B_{mmm}(k_1, k_2, k_3) = 2P(k_1)P(k_2)F_2(k_1, k_2) + 2\text{cyc}, \quad (32)$$

where cyc symbolizes the two cyclic permutations of the k vectors in the power spectrum and mode coupling kernel. From an observational point of view the halo auto bispectrum B_{hhh} is probably the most appealing statistic.

Unfortunately it is suffering from shot noise, which might deviate from its fiducial Poisson form $1/\bar{n}$ [32]. Besides the halo auto power spectrum, there are two halo-matter cross bispectra B_{mhh} and B_{mmh}, where either one or two matter fields are correlated with two or one halo fields, respectively. One further needs to state whether the cross bispectra are symmetrized over the k modes or not.

Our focus is not on observability but on understanding the clustering properties of dark matter halos in N-body simulations and devising a theoretical framework that can later be used to analyze real data. Thus, we will consider the unsymmetrized matter-matter-halo cross bispectrum defined as

$$B_{mmh}^{(unsym)}(k_1, k_2, k_3)(2\pi)^3\delta^{(D)}(k_1 + k_2 + k_3)$$
$$= \langle\delta(k_1)\delta(k_2)\delta_h(k_3)\rangle, \quad (33)$$

where the halo density field is always on the k_3 mode. This particular configuration might not be the one with the highest signal to noise ratio but it has a couple of quite useful properties for our study: (a) The cross bispectrum does not suffer from a spurious shot noise contamination and is thus a clean probe of the clustering of halos and (b) the functional simplicity of the second-order bias contributions in terms of k_1, k_2 and the cosine of the enclosed angle μ where the b_2 and b_{s^2} contributions are basically orthogonal (see below). The latter should allow for a clear distinction between the standard second-order bias picture or its possible extensions discussed above.

As noted above, all of the models under consideration share the same functional form (7) for the second-order halo density field. Only the standard quadratic bias model has $b_{s^2} = 0$. Therefore, we can write down the bispectrum as

$$B_{mmh}^{(unsym)}(k_1, k_2, k_3) - b_1 B_{mmm}(k_1, k_2, k_3)$$
$$= 2P(k_1)P(k_2)\left[b_2 + b_{s^2}\left(\mu^2 - \frac{1}{3}\right)\right]. \quad (34)$$

Note that we use a parametrization where the factors of $1/2$ are absorbed into the bias parameters for simplicity. We will restore these prefactors only at the very end, when we are comparing our bias measurements to the theoretical bias functions. A nonvanishing b_{s^2} in the above equation would be clear evidence for a dynamical biasing picture. After dividing by the two matter power spectra, the remaining quantity is a function of the angle μ only, which simplifies the combination of information from several scales k_1 and k_2.

III. SIMULATIONS AND BISPECTRUM ESTIMATION

A. The simulations

We are studying the cosmic density field in a suite of 11 dark matter only simulations with box size of $L = 1600 \, h^{-1}$Mpc, which are an extension of the simulations described in Ref. [33]. The ΛCDM model is based on

best-fit parameters inferred from the WMAP 5-year data release [34]. Thus, we adopt a mass density parameter $\Omega_m = 0.279$, a baryon density parameter $\Omega_b = 0.0462$, a Hubble constant $h = 0.7$, a spectral index $n_s = 0.96$, and a normalization of the curvature perturbations of $\Delta_{\mathcal{R}}^2 = 2.21 \times 10^{-9}$ at the pivot point $k = 0.02$ Mpc^{-1}. This normalization leads to a present day fluctuation amplitude of $\sigma_8 \approx 0.81$. The initial conditions are set up a redshift $z_i = 99$. The gravitational evolution of the $N_p = 1024^3$ particles is integrated using the publicly available GADGET2 code [35]. The simulation size, particle number and matter density parameter yield a particle mass of $3 \times 10^{11}\ h^{-1} M_\odot$. Dark matter halos are identified using a friends-of-friends halo finder with a linking length of 0.2 times the mean interparticle spacing. Only halos exceeding 20 particles are considered for our analysis, corresponding to a minimum halo mass of approximately $6 \times 10^{12}\ h^{-1} M_\odot$. We consider four mass bins, each spanning a factor of 3 in mass. For the estimation of the statistics, particles are interpolated on a $N_c = 512$ grid using the cloud-in-cell algorithm and the gridded density field is corrected for the window of the grid. The matter-matter-halo and matter bispectrum are measured for low k modes $k < 0.12\ h$Mpc^{-1} in the simulation output at redshift $z = 0$. The bispectrum measurement scales as the sixth power of the number of grid cells per dimension, which makes it computationally very expensive to extract the full bispectrum information at higher k. It would still be interesting to extend the measurement to higher k in the future to determine the scale of breakdown of the tree-level calculation.

B. Bispectrum estimation and data reduction

The bispectrum modes must satisfy the triangle condition $\boldsymbol{k}_1 + \boldsymbol{k}_2 + \boldsymbol{k}_3 = 0$; thus, the shape of the bispectrum is fully specified by two lengths and one angle, which we choose as k_1, k_2 and $\mu = \boldsymbol{k}_1 \cdot \boldsymbol{k}_2 / k_1 k_2$. Since $\delta(\boldsymbol{x})$ is a real valued field, the Fourier modes have to satisfy $\delta^*(\boldsymbol{k}) = \delta(-\boldsymbol{k})$. Consequently, the imaginary part of the bispectrum cancels when we add $\delta(\boldsymbol{k}_1)\delta(\boldsymbol{k}_2)\delta(\boldsymbol{k}_3)$ and $\delta(-\boldsymbol{k}_1)\delta(-\boldsymbol{k}_2)\delta(-\boldsymbol{k}_3)$. We consider bins that are logarithmically spaced in k_1 and k_2 and linearly in μ. We add all the bispectrum amplitudes that fall into the bin centered at (k_1, k_2, μ).

As a first step in our analysis we subtract out the b_1 contribution proportional to the matter bispectrum and divide by the power spectrum measured in the same simulation and k bins to cancel part of the cosmic variance:

$$\hat{M}(k_1, k_2, \mu) = \frac{\hat{B}_{\mathrm{mmh}}^{(\mathrm{unsym})}(k_1, k_2, \mu) - \hat{b}_1 \hat{B}_{\mathrm{mmm}}(k_1, k_2, \mu)}{2\hat{P}_{\mathrm{mm}}(k_1)\hat{P}_{\mathrm{mm}}(k_2)}.$$

(35)

Comparing to Eq. (34), the resulting statistic should be a function of μ only. The hat is used to mark quantities

estimated from the simulations. This quantity is distinct from the usual definition of the reduced bispectrum since the power spectra in the denominator do not depend on k_3 and can thus be controlled by limiting k_1 and k_2. The first-order bias parameter $\hat{b}_1$ is estimated from the halo-matter cross power spectrum on large scales $0.015\ h$Mpc$^{-1} < k < 0.03\ h$Mpc^{-1}, where the linear bias model $P_{\mathrm{hm}} = b_1 P_{\mathrm{mm}}$ is believed to be accurate. We show the k dependence of $\hat{P}_{\mathrm{hm}}(k)/\hat{P}_{\mathrm{mm}}(k)$ and the inferred bias parameters in Fig. 4. Note that the resulting statistic depends only on the magnitude of the k_1 and k_2 modes, so that we can ensure the validity of the perturbative expansion by limiting these modes accordingly.

When showing the reduced data as a function of μ only, we reduce them as follows:

$$\chi_M^2 = \sum_{k_1, k_2} \left(\frac{\hat{M}(k_1, k_2, \mu) - \bar{M}(\mu)}{\Delta M(k_1, k_2, \mu)} \right)^2,$$

(36)

$$\bar{M}(\mu) = \sum_{k_1, k_2} \frac{\hat{M}(k_1, k_2, \mu)}{\Delta M^2(k_1, k_2, \mu)} \left(\sum_{k_1, k_2} \frac{1}{\Delta M^2(k_1, k_2, \mu)} \right)^{-1},$$

(37)

$$\Delta \bar{M}(\mu) = \left(\sum_{k_1, k_2} \frac{1}{\Delta M^2(k_1, k_2, \mu)} \right)^{-1/2}$$

(38)

for each μ.

The cosmic variance of the bispectrum estimates could in principle be measured from the standard deviation between our simulation boxes. Given the small number of boxes this approach is bound to give a very noisy estimate. Since we are using the error for the weighting of the modes, we would like to avoid a spurious upweighting of modes which by chance have a low simulation to simulation variance. For this purpose we prefer a smooth error estimate. As shown in Ref. [36], the variance of the bispectrum is given by

$$\Delta B_{\mathrm{mmh}}^2(k_1, k_2, \mu) = s_{123} \frac{(2\pi)^3 V_f}{V_{123}} P_{\mathrm{mm}}(k_1) P_{\mathrm{mm}}(k_2)$$

$$\times \left(P_{\mathrm{hh}}(k_3) + \frac{1}{\bar{n}_h} \right),$$

(39)

where $V_f = (2\pi)^3/L^3$ is the volume of the fundamental cell, $\bar{n}_h$ is the number density of the tracer and s_{123} takes on values of 1, 2 and 6 for general, isosceles and equilateral triangles, respectively. The norm volume is given by

$$V_{123} = 8\pi^2 k_1^3 k_2^3 (\mathrm{d}\ln k)^2 \mathrm{d}\mu$$

(40)

for our bins, which are logarithmically spaced in k_1 and k_2 and linearly spaced in μ. The above just quantifies the diagonals of the covariance matrix between the different triangle shapes and scales, but the correlations between different triangles are believed to be small [36]. When calculating the error on the reduced bispectrum, we focus

on the error contribution from the matter-matter-halo bispectrum described above and thus have

$$\Delta M(k_1, k_2, \mu) \approx \frac{\Delta B_{\text{mmh}}(k_1, k_2, \mu)}{2 P_{\text{mm}}(k_1) P_{\text{mm}}(k_2)}. \tag{41}$$

This procedure could be clearly improved by modeling or measuring the full covariance matrix.

C. Bias estimation

We can now estimate b_2 and b_{s^2} minimizing

$$\chi^2 = \sum_{k_1, k_2} \sum_{\mu} \left(\frac{\hat{M}(k_1, k_2, \mu) - b_2 L_0(\mu) - b_{s^2} L_2(\mu)}{\Delta M(k_1, k_2, \mu)} \right)^2, \tag{42}$$

where $L_0(\mu) = 1$ and $L_2(\mu) = (\mu^2 - 1/3)$ are the zeroth- and second-order Legendre polynomials, which form an orthogonal set on $[-1, 1]$. The k sums are performed over

$k_{\min} < k_1 < k_{\max}$, $k_{\min} < k_2 < \kappa k_1$ such that $(1 - \kappa) k_1 < k_3 < (1 + \kappa) k_1$ and we use $\kappa = 3/4$ for definiteness.

Defining the cosine

$$\langle a(k_1, k_2, \mu), b(k_1, k_2, \mu) \rangle := \sum_{k_1, k_2} \sum_{\mu} \frac{a(k_1, k_2, \mu) b(k_1, k_2, \mu)}{\Delta M^2(k_1, k_2, \mu)}, \tag{43}$$

we obtain for the best-fit parameters

$$\hat{b}_2 = \frac{\langle L_2, L_2 \rangle \langle L_0, \hat{M} \rangle}{\Delta} - \frac{\langle L_0, L_2 \rangle \langle L_2, \hat{M} \rangle}{\Delta}, \tag{44}$$

$$\hat{b}_{s^2} = -\frac{\langle L_0, L_2 \rangle \langle L_0, \hat{M} \rangle}{\Delta} + \frac{\langle L_0, L_0 \rangle \langle L_2, \hat{M} \rangle}{\Delta}, \tag{45}$$

where $\Delta = \langle L_0, L_0 \rangle \langle L_2, L_2 \rangle - \langle L_0, L_2 \rangle^2$. Note that from χ^2 minimization one obtains an equivalent expression for the cosine of the reduced data:
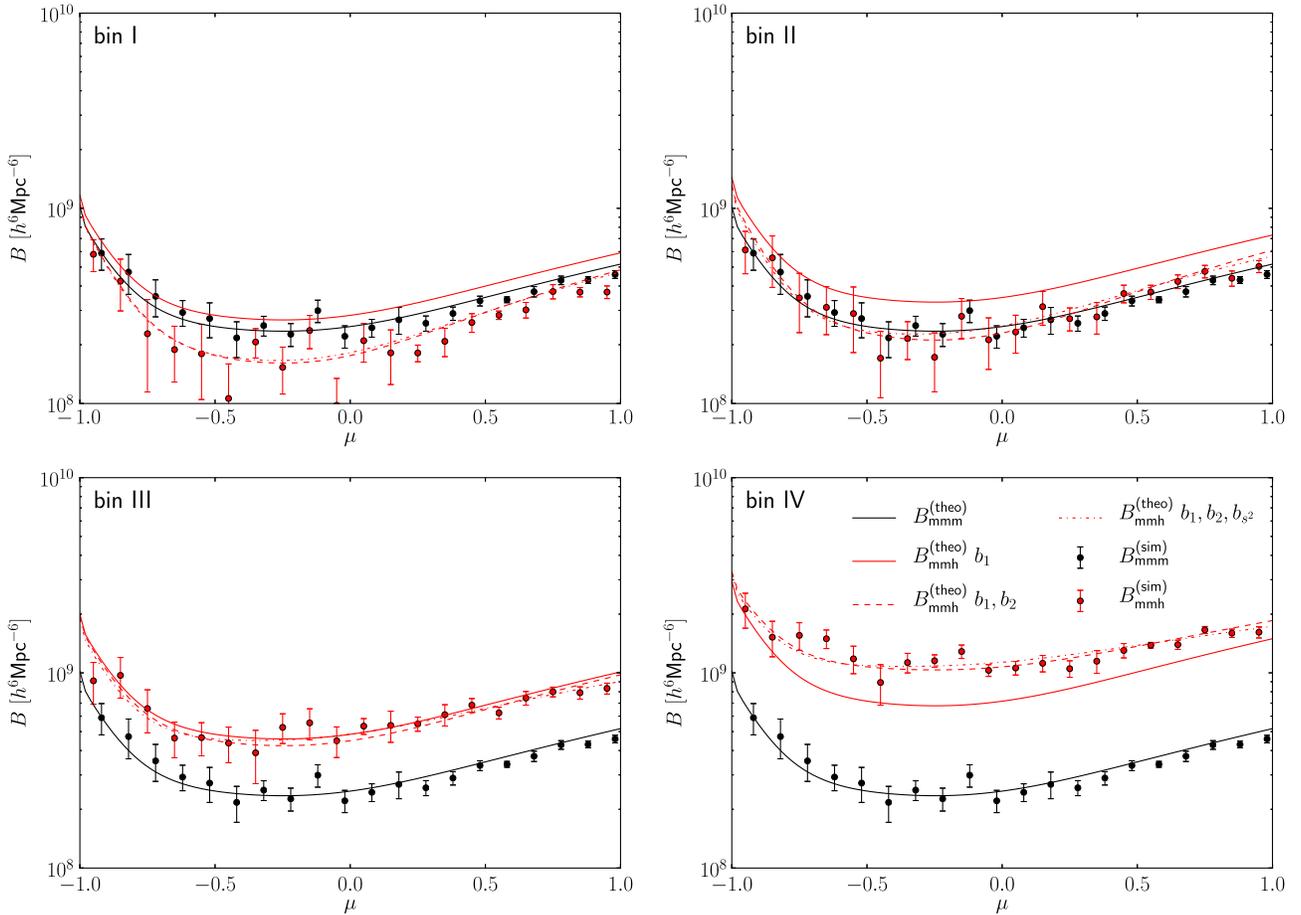

FIG. 1 (color online). Matter (black points) and halo-matter-matter (red points) bispectra as a function of triangle shape for configuration $k_1 = 0.052$ hMpc^{-1}, $k_2 = 0.06$ hMpc^{-1}. The black solid line shows the tree-level prediction for the matter bispectrum, the red solid line has b_1 only and dashed and dashed-dotted lines are adding b_2 and b_{s^2}. The list of bias parameters behind the theoretical cross bispectra in the legend indicates the parameters that were considered for the corresponding curve. The error bars are estimated from the box-to-box variance of the bispectrum measurement. Note that this is only a small fraction of the total bispectrum information that our simulations contain, and the log scale also deemphasizes what are actually significant differences between the fit with and without s^2 (these will be highlighted later).

$$\langle a, b \rangle_\mu := \sum_\mu \frac{a(\mu) b(\mu)}{\Delta \bar{M}^2(\mu)}, \qquad (46)$$

where for $a(\mu)$, $b(\mu)$ we have $\langle a(\mu), M(k_1, k_2, \mu) \rangle = \langle a(\mu), \bar{M}(\mu) \rangle_\mu$ and $\langle a(\mu), b(\mu) \rangle = \langle a(\mu), b(\mu) \rangle_\mu$.

The bias parameter b_1 is estimated from the halo-matter cross power spectrum on large scales and low k, where loop corrections are believed to be unimportant. Furthermore there is no shot noise contamination in the cross power spectrum. We use b_1 measured from the halo-matter cross power spectrum and use it for the bispectrum calculation, because it has a small statistical error. There is a correlation between the b_1 used for the matter bispectrum subtraction and the inferred b_2 and b_{s^2} parameters. The matter bispectrum and the residual considered for our reduced bispectrum should in principle not be degenerate, since the matter bispectrum has additional $L_1(\mu)$ terms and since the coefficients of the three Legendre polynomials in the matter bispectrum depend on the ratio k_2/k_1. However, applying our fitting method to the matter bispectrum we obtain b_2 and b_{s^2} constraints of order unity. Thus an error of Δb_1 in the first-order bias leads to a shift of roughly $-\Delta b_1$ for both b_2 and b_{s^2}. The statistical errors on the second-order bias coefficients are roughly a factor of 5 larger than the statistical error on the corresponding first-order bias, such that this effect is not very important from the statistical point of view. We would only need to worry about it if the first-order bias coefficients in the power spectrum and bispectrum differ. While this may at first glance seem impossible (and it probably is), the higher-order loop terms renormalize b_1 [11] and to our knowledge it has not been explicitly shown that the renormalization works the same way in bispectrum as in power spectrum. In this paper, we will assume that the two are the same.

The errors on the estimated parameters are calculated from the expected deviation in the χ^2. For a n-component parameter vector $\boldsymbol{a}$ the χ^2 in the vicinity of the best-fit parameter set $\hat{\boldsymbol{a}}$ can be described as

$$\chi^2(\boldsymbol{a}) = \chi^2(\hat{\boldsymbol{a}}) + \frac{1}{2} \sum_{i,j} (a_i - \hat{a}_i) \frac{\partial^2 \chi^2}{\partial a_i \partial a_j} (a_j - \hat{a}_j), \qquad (47)$$

where $\Delta \chi^2 = |\chi^2(\boldsymbol{a}) - \chi^2(\hat{\boldsymbol{a}})| = 1$ corresponds to one sigma errors on the parameters. Thus
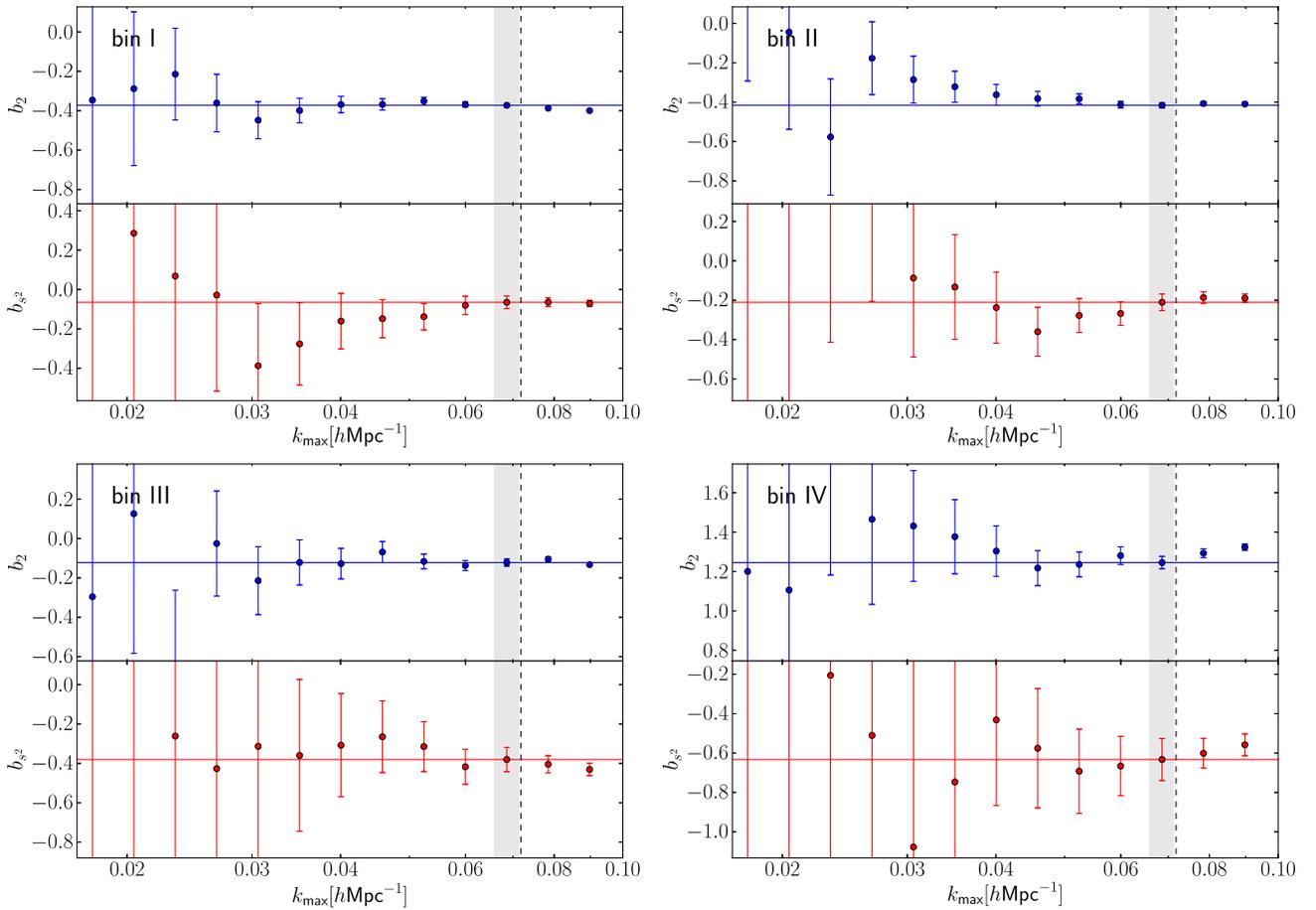

FIG. 2 (color online). Convergence of the measured b_2 (upper panels) and b_{s^2} (lower panels) parameters with increasing maximum k mode for the four mass bins. The horizontal red and blue lines show the constraints obtained for our fiducial $k_{max} = 0.07 \, h\text{Mpc}^{-1}$. The pivot data point is highlighted by the gray shaded region.

$$\Delta b_2 = \sqrt{1/\langle L_0, L_0 \rangle}, \qquad \Delta b_{s^2} = \sqrt{1/\langle L_2, L_2 \rangle}. \qquad (48)$$

We compared these errors with the standard deviation of the bias constraints obtained from the single realizations and found good agreement.

IV. RESULTS

Figure 1 shows the matter bispectrum and matter-matter-halo bispectra for our four mass bins for one configuration of $k_1 = 0.052 \, h\text{Mpc}^{-1}$, $k_2 = 0.06 \, h\text{Mpc}^{-1}$ as a function of the opening angle μ. The matter bispectrum is in quite good agreement with the theoretical prediction in Eq. (32). There is some small tension for positive μ, but this should not be a problem for our study since our bias constraints are not relying on this theoretical modeling since we are subtracting out the matter bispectrum measured from the simulations.

We also plot the matter-matter-halo cross bispectrum and the theoretical model of Eq. (7). To visualize the effect of the contributions of the bias parameters, we plot the

model with vanishing b_2 and b_{s^2}, with vanishing b_{s^2} and the full model. The nonvanishing bias parameters for the theory lines were chosen according to our best-fit model discussed below. While the k values were chosen quite high to reduce the errors, there is still too much scatter in the data points to decide whether the model with and without b_{s^2} gives a better description of the data. This motivated the careful combination of all the information available by weighting the modes accordingly, as described above.

Our main reason to study lowest order nonlinear biasing in the bispectrum was that these terms are the leading-order terms on large scales. As one includes higher momenta, loop corrections gain importance and need to be modeled accordingly. To assess the importance of higher-order corrections and to show the convergence of our fitting procedure, we perform our parameter estimation as a function of the maximum wave number and show the results in Fig. 2. The error bars clearly shrink as we go to higher k and the inferred bias parameters are almost always consistent with our fiducial result shown by the horizontal lines. In these plots we also show the scale up to which we have a
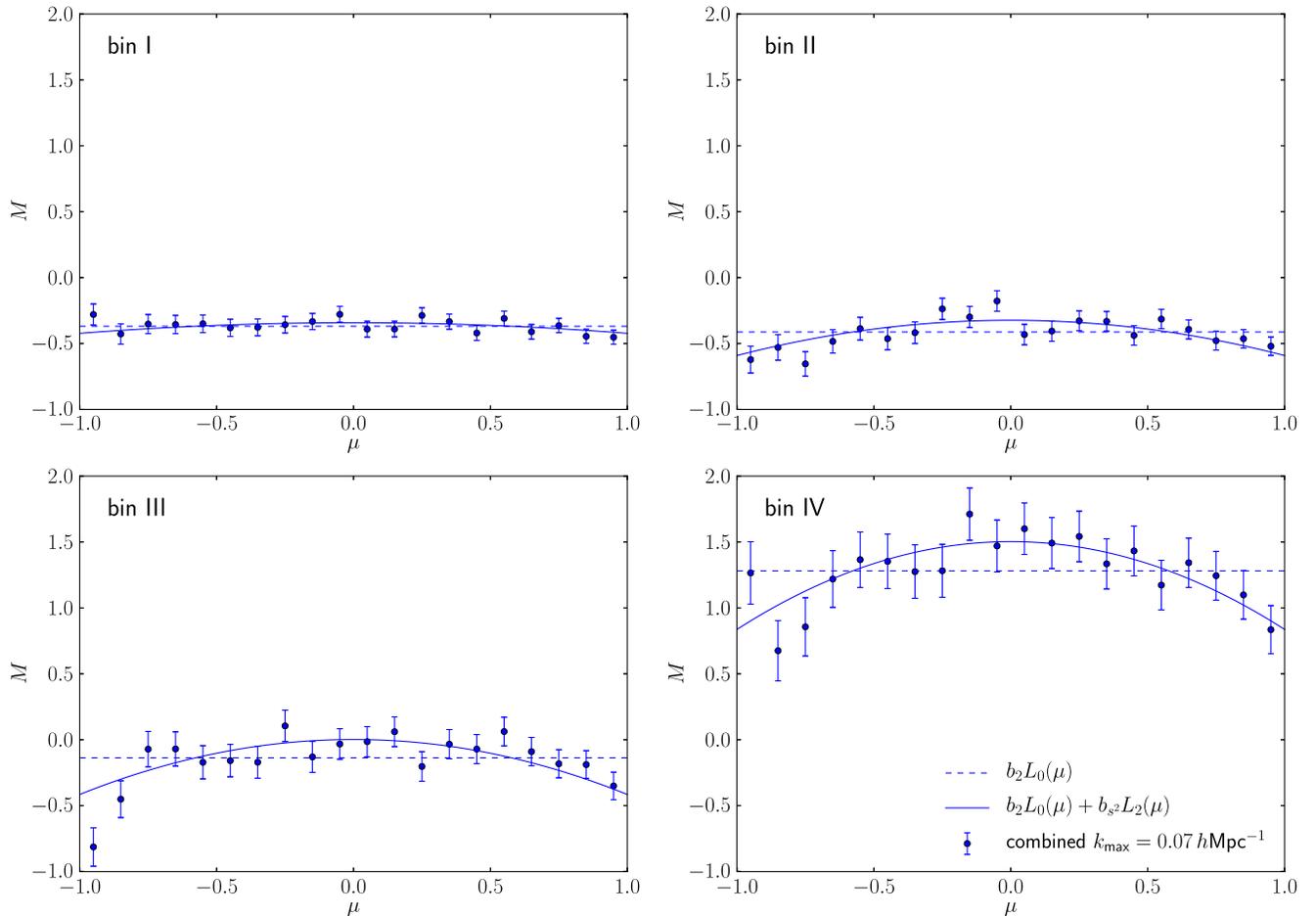

FIG. 3 (color online). Residual shape dependence of the halo bispectrum for our reduced bispectrum defined in Eq. (35). The blue data points with error bars show the result of the combined reduced bispectrum defined in Eq. (37) including all the configurations up to $k_{\text{max}} = 0.07 \, h\text{Mpc}^{-1}$. The horizontal dashed line shows the model including b_2 only, and the solid blue line shows the model including both b_2 and b_{s^2}.

TABLE I. Best-fit bias parameters, their errors and mean mass for our four mass bins. The bias parameters are compared to the theoretical bias functions in Fig. 4. The first-order bias b_1 is extracted from the halo-matter cross power spectrum and the second-order bias parameters are inferred from the cross bispectrum.

	b_1	Δb_1	b_2	Δb_2	b_{s^2}	Δb_{s^2}	$M[h^{-1}M_\odot]$
I	1.142	0.002	-0.37	0.01	-0.07	0.03	9.68×10^{12}
II	1.409	0.002	-0.42	0.01	-0.21	0.04	2.90×10^{13}
III	1.954	0.004	-0.12	0.02	-0.38	0.06	8.58×10^{13}
IV	2.889	0.010	1.25	0.03	-0.63	0.11	2.48×10^{14}

complete measurement of all the modes by the vertical dashed line and highlight the $k_{\max}$ that we use for the primary reported parameter values by the vertical shaded region.

Figure 3 shows our reduced bispectrum $\bar{M}(\mu)$ defined in Eq. (37) as a function of opening angle μ and the combined errors according to Eq. (38). We overplot the b_2-only model and the model including both b_2 and b_{s^2}. These plots show clear evidence for the presence of the tidal term except for the lowest mass bin, for which the b_2-only model gives an acceptable description of the angular dependence.

In Table I, we give the best-fit values of the first- and second-order bias parameters for our four halo mass bins obtained considering all the modes up to $k_{\max} = 0.07 \, h\mathrm{Mpc}^{-1}$. Figure 4 shows the bias parameters as a function of mass together with the corresponding predictions of the spherical collapse model. Note that we are plotting $2\hat{b}_2$, which corresponds to the second-order

Eulerian bias [see Eq. (26)]. The $\hat{b}_1$ measurements from the halo-matter cross power spectrum are in good agreement with the theoretical predictions. The measured $\hat{b}_{s^2}$ are slightly lower than the theoretical predictions for the two central mass bins, but the trend with mass is well reproduced by the theory. The $\hat{b}_2$ measurements are less well reproduced by the theoretical bias function, especially mass bins II and III which are well below the theory. The theoretical predictions for b_1 and b_{s^2} are given by first derivatives of the mass function and do not reproduce the data perfectly. Thus one would naturally expect some corrections for the second derivatives. The disagreement could also be an indication for a failure of the spherical collapse picture at second order. Specifically, the fact that the predicted b_{s^2} disagrees with the measurements suggests that Lagrangian $b_{s^2}^{(\mathrm{L})}$ is not zero, as predicted by the ellipsoidal collapse model [26–29].

The right panel of Fig. 4 shows the ratio of halo-matter and matter-matter power spectra used for the inference of the first-order bias. We are fitting for $\hat{b}_1$ on large scales to avoid the regime where the nonlinear corrections become important. These corrections are affecting the highest mass bin quite strongly already starting at $k \approx 0.05 \, h\mathrm{Mpc}^{-1}$. The corrections are stronger for higher mass objects, in accordance with the general mass dependence of the second-order bias parameters derived here, but a full discussion of all the terms entering at one-loop level must also include the third-order terms, which is beyond the scope of this paper.

As in the power spectrum analysis, the bispectrum is increasingly affected by loop corrections as one increases the maximum momentum in the problem. The relevant quantity here is the largest external momentum involved
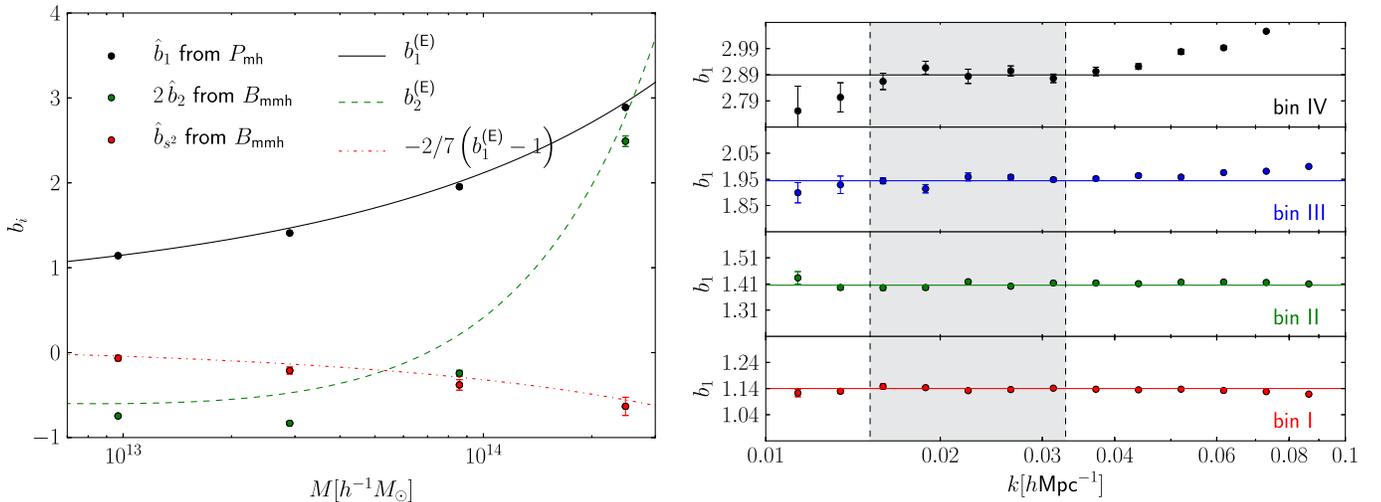

FIG. 4 (color online). *Left panel*: Mass dependence of the bias parameters and theoretical predictions. The points with error bars are our best-fit parameters for $\hat{b}_1$, $2\hat{b}_2$ and $\hat{b}_{s^2}$. The numerical values of the data points are given in Table I. The curves show the corresponding theoretical bias functions as calculated using the relations in Sec. II E. The measurements for $\hat{b}_1$ are in good agreement with the theory; there is a clear deviation for the $\hat{b}_{s^2}$ and $\hat{b}_2$ measurement for the two central mass bins. *Right panel*: Ratio of the simulation halo matter and matter power spectra $\hat{P}_{\mathrm{hm}}(k)/\hat{P}_{\mathrm{mm}}(k)$ and first-order bias parameters inferred using the data points highlighted by the shaded region.

and thus one should make sure that all the k's are in the perturbative regime and can be well described by the order of perturbation theory considered. Our study focuses on the large scale bispectrum, where a tree-level treatment should be sufficiently accurate and we have shown that the constraints are both stable and consistent as we increase $k_{\max}$ up to $0.1\ h\mathrm{Mpc}^{-1}$. Extensions of the perturbative treatment further into the nonlinear regime might be possible based on clipping techniques [37].

V. DISCUSSION AND OUTLOOK

In this paper, we presented a dynamical motivation for the second-order tidal tensor bias term proposed in Ref. [5], showing that it is naturally generated by gravity even if absent in the initial conditions. We performed a measurement of this bias for dark matter halos in simulations, showing clear evidence for the tidal tensor bias, increasing with the halo mass. Our results are consistent with the picture in which a significant part of the tidal tensor bias is generated by the gravitational evolution, but we also find some evidence that it is present already in the initial conditions. While the functional form of the additional terms agrees with the discussion in Ref. [5] the dynamical derivation can supplement it by a prediction of the time dependence and gives at least qualitative understanding about the mass dependence of the bias parameters.

Our analysis also includes second-order density bias b_2, which we find to disagree with the theoretical predictions at a quantitative level, even if it qualitatively follows the predictions that it should be negative at low mass and increase with halo mass. The disagreement calls for a reinvestigation and improvement of the theoretical bias function or measurement of the second-order bias parameters in the initial conditions, where the Lagrangian bias parameters are postulated to describe the density field of the protohalos. The deviation between the theoretical and measured b_2 parameters does not necessarily mean that the Lagrangian picture is wrong, but rather that the bias functions derived from the spherical collapse model and the mass function might not be sufficiently accurate.

Because these two terms are quadratic, they contribute a loop correction to the power spectrum, so the standard linear bias picture still applies on very large scales, even if they contribute at the leading order to the bispectrum. If we want to understand the halo power spectrum on smaller scales, then the loop corrections caused by these quadratic terms become important. However, a consistent calculation of the halo correlation function or power spectrum at one-loop level requires a model of the halo density field up to third order, including all the nonlocal terms [5]. This gives rise to several other terms that contribute to the power spectrum at the same order, each with a prefactor that may depend on the halo mass. A clean extraction of these nonlinear bias coefficients from the power spectrum alone is very difficult and instead higher-order correlations are needed to separate these terms. This paper is a first step in extracting the quadratic coupling terms from the bispectrum. The next step in this program is to extract the cubic-order terms from the trispectrum: such an analysis will be presented elsewhere. For this reason a discussion of the implications on the two-point function based on our results for the quadratic couplings cannot be complete. Still, there are some obvious implications of our results. One is that the nonlocal tidal tensor bias contributions must be included in the analysis of galaxy power spectrum and ignoring them may lead to incorrect conclusions. This effect is specially relevant for the broadband power but will also have an effect on the position of the baryonic acoustic oscillations (BAO), just like the quadratic density term does if $b_2 \neq 0$ [38,39]. Our calculation in Appendix B shows that this effect is subdominant, with about a factor of 4 lower prefactor in front of b_{s^2} relative to the b_2 term, suggesting it will not strongly affect the measurement of the true BAO scale.

APPENDIX A: MATTER DENSITY IN LPT UP TO SECOND ORDER

In the above derivation of the final halo density field arising from a local bias in Lagrangian space we used the Lagrangian displacement field and the second-order matter density in SPT. In Ref. [40], it is shown that after expanding the exponential damping prefactor, the one-loop power spectra in LPT and SPT are identical. This Appendix shows that this equivalence is true also in terms of the fields *if* one expands the LPT expressions up to the desired order in the density field. Without these expansions, LPT was shown to contain a nontrivial resummation of SPT terms.

For nth order displacement field one has [40]

$$
{}^{(n)}\boldsymbol{\psi}(\boldsymbol{k},\eta) = -\frac{\mathrm{i}}{n!}\int\frac{\mathrm{d}^3 p_1}{(2\pi)^3}\cdots\int\frac{\mathrm{d}^3 p_n}{(2\pi)^3}\,{}^{(n)}\boldsymbol{L}(\boldsymbol{p}_1,\ldots,\boldsymbol{p}_n)
$$
$$
\times\,\delta(\boldsymbol{p}_1,\eta)\ldots\delta(\boldsymbol{p}_n,\eta)(2\pi)^3\delta^{(\mathrm{D})}\!\Big(\boldsymbol{k}-\sum\boldsymbol{p}_i\Big),
$$

(A1)

with the kernels

$$^{(1)}L(p) = \frac{p}{p^2},$$

$$^{(2)}L(p_1, p_2) = \frac{3}{7} \frac{p_1 + p_2}{|p_1 + p_2|^2} \left[1 - \left(\frac{p_1 \cdot p_2}{p_1 p_2} \right)^2 \right]. \tag{A2}$$

The density field in k space can be obtained upon Fourier transforming the Eulerian field in configuration space and using the Jacobian mapping $[1 + \delta(x, \eta)]d^3x = d^3q$:

$$\delta(k, \eta) = \int d^3q \exp[ik \cdot q]\{\exp[ik \cdot \psi(q, \eta)] - 1\}. \tag{A3}$$

We can now expand the exponential up to second order in the displacement field

$$\delta(k, \eta) \approx \int d^3q \exp[ik \cdot q]\Big\{ik \cdot \psi(q, \eta)$$
$$- \frac{1}{2}(k \cdot \psi(q, \eta))^2\Big\} \tag{A4}$$

$$= ik \cdot {}^{(1)}\psi(k, \eta) + ik \cdot {}^{(2)}\psi(k, \eta)$$
$$+ \frac{1}{2} \int \frac{d^3k'}{(2\pi)^3} \frac{k \cdot k'}{(k')^2} \frac{k \cdot (k - k')}{|k - k'|^2}$$
$$\times {}^{(1)}\delta(k', \eta){}^{(1)}\delta(k - k', \eta) \tag{A5}$$

$$= {}^{(1)}\delta(k, \eta) + \int \frac{d^3k'}{(2\pi)^3}$$
$$\times F_2(k', k - k'){}^{(1)}\delta(k', \eta){}^{(1)}\delta(k - k', \eta). \tag{A6}$$

Thus, expanding the exponential we see that LPT and SPT agree at second order in the density field.

APPENDIX B: ON SHIFTS IN THE BAO

As shown recently in Ref. [39] and discussed before in Ref. [41], second-order bias terms lead to a distinct shift in the position of the BAO feature. In this Appendix, we generalize their calculation to account also for the shift due to the tidal tensor bias.

Let us start by generalizing the mode coupling kernel to biased tracers. The structure of the quadratic and tidal tensor terms in the second-order halo density field in Eq. (14) suggests the following functional form:

$$F_{2,h}(q_1, q_2) = b_1 F_2(q_1, q_2) + b_2 + b_{s^2} S_2(q_1, q_2). \tag{B1}$$

With this definition, the second-order halo density field can be written as

$$^{(2)}\delta_h(k) = \int \frac{d^3q_1}{(2\pi)^3} \int \frac{d^3q_2}{(2\pi)^3}$$
$$\times F_{2,h}(q_1, q_2){}^{(1)}\delta(q_1){}^{(1)}\delta(q_2)\delta^{(D)}(k - q_1 - q_2), \tag{B2}$$

and the mode coupling power spectrum is given by

$$P_{hh,22}(k) = \int \frac{d^3q_1}{(2\pi)^3} \int \frac{d^3q_2}{(2\pi)^3} F_{2,h}^2(q_1, q_2)P(q_1)$$
$$\times P(q_2)\delta^{(D)}(k - q_1 - q_2). \tag{B3}$$

When considering the full one-loop halo power spectrum, there is also a contribution from the coupling between linear and cubic halo density field, the term corresponding to the propagator $P_{13}(k)$ in the matter power spectrum. This term does not contribute to the shift of the BAO and can thus be neglected for our arguments here, except for a cancellation to be discussed below.

For the BAO shift, we are interested in the effect of long wavelength modes ($q \ll \Lambda$) on the correlation function around the BAO scale, where $1/\Lambda$ is a cutoff wavelength exceeding the scales of interest. Thus, we need to consider the high-k limit of the above integral, corresponding to $q_1 \ll k$ and $q_2 \ll k$:

$$P_{hh,22}(k) \overset{k \gg \Lambda}{\approx} \left[\frac{569}{735}b_1^2 + \frac{52}{21}b_1b_2 + 4b_2^2 \right.$$
$$\left. - \frac{272}{315}b_1b_{s^2} + \frac{16}{45}b_{s^2}^2 \right]P(k)\sigma_1^2 + k^2P(k)\sigma_{v,1}^2$$
$$+ \left[\frac{47}{105}b_1^2 + \frac{4}{3}b_1b_2 + \frac{16}{45}b_1b_{s^2} \right]kP'(k)\sigma_1^2$$
$$+ \frac{1}{10}b_1^2k^2P''(k)\sigma_1^2, \tag{B4}$$

where $\sigma_1^2 = \int_0^\Lambda \frac{d^3q}{(2\pi)^3}P(q)$ is the variance of the long wavelength modes and $\sigma_{v,1}^2 = \int_0^\Lambda \frac{d^3q}{(2\pi)^3}P(q)/3q^2$ is the velocity dispersion of the long wavelength displacement field. The $k^2P(k)\sigma_{v,1}^2$ term is canceled by the propagator $P_{hh,13}$ in the high-k regime and can thus be neglected in the following. Using the following two Fourier transform (FT) relations between the correlation function and power spectrum, FT$[kP'(k)] = -r\xi'(r) - 3\xi(r)$ and FT$[k^2P''(k)] = r^2\xi''(r) + 8r\xi'(r) + 12\xi(r)$, we obtain for the correlation function in the presence of a long wavelength mode

$$\xi_{hh,s}(r) \approx b_1^2\xi(r) + \left[\frac{356}{147}b_1^2 + \frac{80}{21}b_1b_2 - \frac{32}{63}b_1b_{s^2} \right.$$
$$\left. + 4b_2^2 + \frac{16}{45}b_{s^2}^2 \right]\xi(r)\sigma_1^2 + \left[\frac{131}{105}b_1^2 + \frac{4}{3}b_1b_2 \right.$$
$$\left. + \frac{16}{45}b_1b_{s^2} \right]r\xi'(r)\sigma_1^2 + \frac{1}{10}b_1^2r^2\xi''(r). \tag{B5}$$

Here we have added in the linear correlation function of the halos, $b_1^2\xi(r)$.

Finally, we have for the shift term proportional to $r\xi'(r)$:

$$\frac{131}{105}b_1^2\sigma_1^2\left(1 + \frac{140}{131}\frac{b_2}{b_1} + \frac{112}{393}\frac{b_{s^2}}{b_1} \right)r\xi'(r). \tag{B6}$$

Let us discuss the relevance of the shift terms based on the mass dependence of the bias parameters depicted in Fig. 4. For halos with $M < 10^{14} h^{-1}M_\odot$ the b_{s^2} effect has the same sign as the b_2 effect, whereas they cancel partially

for higher mass objects. On the other hand b_{s^2} is parametrically smaller than b_2 for most of the considered mass range and even if the bias parameters were of the same magnitude, the prefactors in Eq. (B6) lead to a factor of 4 stronger contribution from the quadratic bias term. Thus, we conclude that the tidal tensor term only leads to a small shift correction on top of the already small correction due to quadratic bias.

[1] M. J. Rees and J. P. Ostriker, Mon. Not. R. Astron. Soc. **179**, 541 (1977).

[2] S. D. M. White and M. J. Rees, Mon. Not. R. Astron. Soc. **183**, 341 (1978).

[3] N. Kaiser, Astrophys. J. **284**, L9 (1984).

[4] J. N. Fry and E. Gaztanaga, Astrophys. J. **413**, 447 (1993).

[5] P. McDonald and A. Roy, J. Cosmol. Astropart. Phys. 08 (2009) 020.

[6] J. A. Frieman and E. Gaztanaga, Astrophys. J. **425**, 392 (1994).

[7] S. Matarrese, L. Verde, and A. F. Heavens, Mon. Not. R. Astron. Soc. **290**, 651 (1997).

[8] A. Buchalter and M. Kamionkowski, Astrophys. J. **521**, 1 (1999).

[9] E. Gaztañaga and R. Scoccimarro, Mon. Not. R. Astron. Soc. **361**, 824 (2005).

[10] M. Manera and E. Gaztañaga, Mon. Not. R. Astron. Soc. **415**, 383 (2011).

[11] P. McDonald, Phys. Rev. D **74**, 103512 (2006).

[12] N. Roth and C. Porciani, Mon. Not. R. Astron. Soc. **415**, 829 (2011).

[13] J. E. Pollack, R. E. Smith, and C. Porciani, Mon. Not. R. Astron. Soc. **420**, 3469 (2012).

[14] J. M. Bardeen, J. R. Bond, N. Kaiser, and A. S. Szalay, Astrophys. J. **304**, 15 (1986).

[15] S. L. Lumsden, A. F. Heavens, and J. A. Peacock, Mon. Not. R. Astron. Soc. **238**, 293 (1989).

[16] V. Desjacques, M. Crocce, R. Scoccimarro, and R. K. Sheth, Phys. Rev. D **82**, 103529 (2010).

[17] A. Elia, A. D. Ludlow, and C. Porciani, Mon. Not. R. Astron. Soc. **421**, 3472 (2012).

[18] R. Takahashi, Prog. Theor. Phys. **120**, 549 (2008).

[19] P. Catelan, C. Porciani, and M. Kamionkowski, Mon. Not. R. Astron. Soc. **318**, L39 (2000).

[20] F. R. Bouchet, R. Juszkiewicz, S. Colombi, and R. Pellat, Astrophys. J. Lett. **394**, L5 (1992).

[21] A. Elia, S. Kulkarni, C. Porciani, M. Pietroni, and S. Matarrese, Mon. Not. R. Astron. Soc. **416**, 1703 (2011).

[22] A similar approach was presented by R. Scoccimarro, in Proceedings of the PTchat workshop, Saclay (unpublished).

[23] F. Bernardeau, S. Colombi, E. Gaztanaga, and R. Scoccimarro, Phys. Rep. **367**, 1 (2002).

[24] J. N. Fry, Astrophys. J. **461**, L65 (1996).

[25] R. Scoccimarro, R. K. Sheth, L. Hui, and B. Jain, Astrophys. J. **546**, 20 (2001).

[26] S. D. M. White and J. Silk, Astrophys. J. **231**, 1 (1979).

[27] J. R. Bond and S. T. Myers, Astrophys. J. Suppl. Ser. **103**, 1 (1996).

[28] R. K. Sheth, H. J. Mo, and G. Tormen, Mon. Not. R. Astron. Soc. **323**, 1 (2001).

[29] V. Desjacques, Mon. Not. R. Astron. Soc. **388**, 638 (2008).

[30] R. K. Sheth and G. Tormen, Mon. Not. R. Astron. Soc. **308**, 119 (1999).

[31] U. Seljak and M. S. Warren, Mon. Not. R. Astron. Soc. **355**, 129 (2004).

[32] N. Hamaus, U. Seljak, V. Desjacques, R. E. Smith, and T. Baldauf, Phys. Rev. D **82**, 043515 (2010).

[33] V. Desjacques, U. Seljak, and I. T. Iliev, Mon. Not. R. Astron. Soc. **396**, 85 (2009).

[34] E. Komatsu et al. (WMAP Collaboration), Astrophys. J. Suppl. Ser. **180**, 330 (2009).

[35] V. Springel, Mon. Not. R. Astron. Soc. **364**, 1105 (2005).

[36] R. Scoccimarro, E. Sefusatti, and M. Zaldarriaga, Phys. Rev. D **69**, 103513 (2004).

[37] F. Simpson, J. B. James, A. F. Heavens, and C. Heymans, Phys. Rev. Lett. **107**, 271301 (2011).

[38] N. Padmanabhan and M. White, Phys. Rev. D **80**, 063508 (2009).

[39] B. D. Sherwin and M. Zaldarriaga, Phys. Rev. D **85**, 103523 (2012).

[40] T. Matsubara, Phys. Rev. D **77**, 063530 (2008).

[41] N. Padmanabhan and M. White, Phys. Rev. D **80**, 063508 (2009).

[42] K. C. Chan, R. Scoccimarro, and R. K. Sheth, Phys. Rev. D **85**, 083509 (2012).